Atomistic insights into early stage corrosion of bcc Fe surfaces in oxygen dissolved liquid lead-bismuth eutectic (LBE-O)

Ting Zhou(周婷)[1,2], Xing Gao(高星)[1,2,†], Zhiwei Ma(马志伟)[1,2], Hailong Chang(常海龙)[1,2], Tielong Shen(申铁龙)[1,2], Minghuan Cui(崔明焕)[1,2], and Zhiguang Wang(王志光)[1,2,†]

[1] *Institute of Modern Physics, Chinese Academy of Sciences, Lanzhou* 730000, *China*
[2] *School of Nuclear Science and Technology, University of Chinese Academy of Sciences, Beijing* 100049, *China*

(Received 6 June 2022; revised manuscript received 12 July 2022; accepted manuscript online 22 July 2022)

Classical molecular dynamics simulations with global neural network machine learning potential are used to study early stage oxidation and dissolution behaviors of bcc Fe surfaces contacting with stagnant oxygen dissolved liquid lead-bismuth eutectic (LBE-O). Both static and dynamic simulation results indicate that the early stage oxidation and dissolution behaviors of bcc Fe show strong orientation dependence under the liquid LBE environments, which may explain the experimental observations of uneven interface between iron-based materials and liquid LBE. Our investigations show that it is the delicate balance between the oxide growth and metal dissolution that leads to the observed corrosion anisotropy for bcc Fe contacting with liquid LBE-O.

Keywords: liquid lead-bismuth eutectic (LBE), global neural network (G-NN) potential, dissolution

PACS: 68.08.–p, 28.41.Qb, 28.52.Fa, 28.52.Av **DOI:** 10.1088/1674-1056/ac834b

1. Introduction

Interest in dissolution and oxidation of iron surfaces originates from its importance in both elementary mechanisms and technological applications such as corrosion and metallurgy. In particular, orientation-dependent surface oxidation behavior is important to guide surface engineering in terms of corrosion resistance of materials. Iron-based materials with excellent corrosion tolerance are in urgent demand for safe operation of future generation-IV systems, such as super-critical water reactor, very high temperature reactor, and lead-cooled fast reactor (LFR). The atmosphere under these reactors, either wet or dry, will lead to the oxidation or dissolution of the iron-based materials. Studies on interactions between different electrolytes or high temperature gases and different oriented iron-based alloy surfaces have been undertaken by several groups.[1–8] Roughly speaking, studies on iron-based alloys contacting with different electrolytes[5–8] show that corrosion behaviors of alloys are strongly dependent on their crystallographic orientations, and these crystal orientation-dependent corrosion behaviors are apparently related to the surface atomic packing pattern and its density.

Liquid lead-bismuth eutectic (LBE) (44.5 wt.% Pb+55.5 wt.% Bi) appears to be the primary candidate coolant for the LFR because of its excellent thermal-physical and chemical properties, including low melting point of 397 K, rapid heat dissipation of the target, considerable neutron yield, and low vapor pressure.[9] However, both austenitic and ferritic-martensitic steels, which are the main candidate structural materials for LFRs, are severely corroded by the liquid LBE if they are exposed directly to liquid LBE at medium to high temperatures. Therefore, compatibility of iron-based materials with LBE in terms of corrosion is an important issue in selections of appropriate structural materials and operating parameters for LFR.[10] An extensive amount of work on corrosion behaviors of both austenitic and ferritic-martensitic steels in liquid LBE have been reported.[11–17] In order to ensure sufficient corrosion resistance of iron-based materials during expected service lifetime, active oxygen control to promote and maintain a protective film is a method developed to mitigate liquid metal corrosion of iron-based materials. It has been elucidated[18] that a passive film on steel surface can effectively prevent the liquid metal embrittlement (LME). Moreover, a passive film is also of great significance to act as diffusion barriers against the dissolution of structural elements into liquid LBE and liquid LBE penetration into a metal substrate.[19] However, due to insufficient control of the key testing parameters and different experimental procedures implemented in different labs, existing corrosion data obtained by examination of corrosion layers after exposure of steels to LBE at similar conditions show significant scatter of the results.[12,19,20] Therefore, structural and kinetic insights into underlying processes of Fe surface exposed to liquid LBE are critical to understand the corrosion mechanism and obtain a passive film to figure out an effective way to enhance its corrosion resistance.

Although the corrosion mechanism of alloys in liquid metals cannot simply be classified as electrochemical or high temperature corrosion, it has been concluded that the corro-

†Corresponding author. E-mail: xinggao@impcas.ac.cn
‡Corresponding author. E-mail: zhgwang@impcas.ac.cn
© 2023 Chinese Physical Society and IOP Publishing Ltd

sion behavior of steels in oxygen dissolved stagnant liquid LBE mainly contains two forms: dissolution and oxidation. In terms of dissolution, it means either dissolution of structural elements into liquid LBE or penetration of liquid LBE component into the metal substrate. It directly degrades the integrity of the base metal and its rate tends to increase with temperatures at low oxygen concentration. In the case of the oxidation, on the one hand, the thermohydraulic problem can be caused by the decreased heat removal capability due to the excess oxidation at the elevated temperatures and high oxygen concentrations. On the other hand, a continuous, slow growing, thermochemically stable and well adherent passive film is advantageous to corrosion protection. However, experimental results[21] have indicated that the presence of liquid LBE-O brings about a very different oxidation process compared with the oxidation in gaseous or aqueous environment. First, the oxidation rate could be reduced because of the much slower oxygen supply in the liquid LBE as compared to the gaseous or aqueous environment. Second, the presence of liquid LBE could increase the diffusion rate of the metal elements through the oxide layer and result in the enhanced oxidation rate. Moreover, the dissolution process of Fe in LBE-O is expected to be different from those in electrochemical corrosion cases. Despite these differences, the oxidation and dissolution of alloy surfaces are essentially related to the atomic packing on the surfaces. Thus, orientation dependence of oxidation and dissolution as Fe exposed to liquid LBE-O should be as crucial as exposed to electrolyte or gases. However, limited by experimental technique and the almost instantaneous time scale of oxidation process, research on influences of the crystal orientation is rare under the liquid LBE environment.

Computer simulation plays an indispensable role in modern materials science research and gets more and more important due to the explosive growth of supercomputing capacity. It not only supplements experimental investigations, but also can guide experiments to some extent. As for the corrosion behavior of Fe in liquid LBE, Xu *et al.*[22] calculated different kinds of energies to estimate the possibilities of absorptions of adatoms (Pb, Bi and Au) and formations of vacancies (or escaped Fe atoms) on the Fe(100), (110) and (111) surfaces. However, these first-principles calculations are confined to very small system sizes and do not include the effect of temperatures. Hence the dynamics associated with the oxide growth on metal surface under liquid LBE-O environment may not be adequately modeled by these approaches. Molecular dynamics (MD) simulations on metal corrosion can provide valuable complementary tool to investigate both the dissolution and oxidation characteristics of metals at nanometer length scales.[23,24] Nevertheless, the high-accuracy *ab initio* simulations cost computationally high, and the classical MD simulations of corrosion of stainless steels by liquid LBE-O are of challenge due to the lack of precise interatomic potential describing the interactions among lead, bismuth, oxygen and alloying atoms. In the meantime, machine learning approach has been able to compromise these two numerical techniques. Instead of solving the Schrödinger equation directly, the machine learning based simulations rely on a large data set of *ab initio* potential energy surfaces (PESs) and complex numerical models.[25,26] Here, we demonstrate, using global neural network (G-NN) machine learning potential molecular dynamics simulations, the influence of crystallographic orientation on the dissolution and oxidation behaviors of bcc Fe surfaces contacting with oxygen dissolved liquid lead-bismuth eutectic. Within the time scale (nanoscale) applicable to molecular dynamics, we specifically report on the early stage oxidation and dissolution behaviors of bcc Fe surfaces contacting with liquid LBE-O. In addition, first-principles method has been employed to verify accuracy of the G-NN potential and help account for some of the MD simulation results.

2. Modeling

All dynamic simulations in this study were performed by using classical MD method as implemented in the LAMMPS package.[27] Different low index bcc Fe surface-liquid LBE-O interfaces were constructed to simulate the behaviors of Fe, Pb, Bi and O atoms at the typical steel-liquid LBE interface region. The interatomic interactions in this quaternary system were described by the G-NN potential (released at www.lasphub.com), which was constructed by global potential energy surface exploration.[25] Particularly, the Fe–Pb–Bi–O quaternary G-NN potential contains 444 power-type structural descriptors (PTSDs) for each element, i.e., 156 two-body PTSDs, 270 three-body PTSDs, and 18 four-body PTSDs, and the network involves two hidden layers and each layer contains 50 neurons (444-50-50-1 net). The final Fe–Pb–Bi–O global dataset consists of 19700 structures covering metallic Fe, Pb, Bi, their compounds and oxides with various stoichiometries. The final root-mean-square (rms) errors of energy and force are 4.428 meV per atom and 0.117 eV/Å, respectively. We should, however, emphasize that the computational cost of the G-NN with the current implementation is about 2–3 orders of magnitude higher than traditional analytical potentials. The high computational cost makes it difficult to conduct too large system simulation, so the total number of atoms simulated in this study is about 5000.

For the dissolution and oxidation behavior simulation of clean bcc Fe(100) surface exposed to liquid LBE, a metal slab comprised of a $12\times12\times12$ conventional body-centered cubic (bcc) unit cells with lattice constant of 2.835 Å terminated by the (100) surface. The $12\times12\times12$ cell without vacuum was first equilibrated using NPT MD simulations. A snapshot from this equilibrium run with an instantaneous unit cell length was

chosen as the starting crystal for interface construction. Similar procedures were performed for the (110) and (111) surfaces. Then, separate samples of liquid LBE-O containing 550 Bi atoms, 450 Pb atoms and 22 O atoms were equilibrated using NPT MD with fixed *xy* cross-sectional dimensions to match the cross section of (100), (110) or (111) surfaces, respectively. It is noted that the oxygen concentration of our simulated system is higher than the saturation oxygen concentration in the liquid LBE measured by the experiment due to the limitation of simulations. The interface was assembled by conjoining the Fe slabs and liquid LBE-O at their common cross sections and applying periodic boundary conditions to the conglomerate with vacuum of 15 Å along *z* axis. An initial gap of 1.5 Å between the Fe surface and liquid LBE was used to mitigate the effect of high-energy interactions generated by too close distance of different types of atoms at the interface. Figure 1 shows the model of the clean bcc Fe(100) and liquid LBE-O.

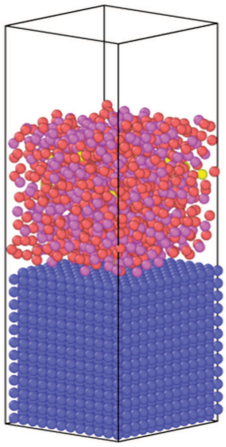


Fig. 1. Model of typical bcc Fe(100)-liquid LBE-O (red, pink, yellow and blue balls represent Bi, Pb, O and Fe atoms, respectively.)

After assembling the interface, we have performed short simulations in isothermal-isobaric ensemble (NPT) to adjust the whole system, and long simulations in canonical ensemble (NVT) to simulate the interaction between the bcc Fe and liquid LBE-O with time step of 1 fs. The NVT production runs lasted 2000000 time steps, totally 2 ns, similar to the time length used in other chemically heterogeneous MD simulations.[28] The simulations were under temperature of 873 K. Due to the timescale limitation of MD simulation, the number of O atoms that could travel from liquid LBE to Fe substrate side is relatively small. In consequence, it is hard to get thorough insight into the synergistic interaction of oxidation and dissolution of the surface in the liquid LBE-O in nanosecond timescale simulations. Therefore, we have conducted additional simulations with oxygen precovered surfaces contacting with LBE-O at the beginning of the simulations. The configurations for oxygen-precovered systems are modeled similarly to that of the clean Fe surfaces except randomly adding oxygens to the surfaces in advance. Our analysis was carried out with OVITO and other home-made software based on LAMMPS' pizza.py toolkit.

3. Results

3.1. Characteristic parameters of Fe surfaces and liquid LBE-O

Characteristic parameters of bulk Fe and its surfaces and oxygen dissolved liquid LBE are determinant to simulate the early stage oxidation and dissolution of bcc Fe exposed to liquid LBE-O. Meanwhile, it is important to verify the accuracy of the state-of-the-art machine-learning interatomic potential used in this work before further simulations. Table 1 provides the lattice constant calculated by the present G-NN potential, which agrees well with DFT calculations and is slightly lower than the experimental result.

Table 1. Lattice constant (Å) of bcc Fe.

G-NN potential	DFT (present)	DFT[29]	Experiment[30]
2.835	2.830	2.842	2.8665

Surface energy and adsorption energy of a clean surface are important parameters to interpret both the dissolution and oxidation behaviors of the surface. The surface energy γ can be calculated by the following equation:[31]

$$\gamma = \frac{1}{2A} \times (E_{\text{slab}} - E_{\text{bulk}}), \tag{1}$$

where A is the surface area, E_{slab} is the total energy of the slab, and E_{bulk} is the total energy of bulk with the same number of atoms.

First, as shown in Table 2, the G-NN potential predicts that the bcc Fe(110) surface is the most stable one, followed by the (100) surface, then (111) surface, which is consistent with both the DFT results and the experimental results. It is noted that difference between the Fe(100) surface and (110) surface is minor, and the surface energy of the Fe(111) surface is much higher due to its lower atomic density. These different surface atomic densities will have significant effects on the dissolution and oxidation behaviors of these surfaces.

Table 2. Surface energies (J/m^2) of bcc Fe(100), Fe(110), and Fe(111).

	G-NN potential	DFT(present)	ReaxFF[32]	Experiment[33]
Fe(100)	2.31	2.48	2.46	
Fe(110)	2.25	2.42	2.41	2.41
Fe(111)	2.43	2.70	2.71	

It is well known that corrosion is also closely related to surface adsorption and other chemical reactions that may happen in certain corrosive environment. The adsorption energies of an adatom on different Fe surfaces at different sites have been calculated according to the following formula:[22]

$$E_{\text{ads}} = E_{\text{slab}}^{\text{ads}} - E_{\text{slab}} - E^{\text{ads}}. \tag{2}$$

Here, E^{ads}_{slab} and E_{slab} are the total energies of the Fe slab with and without an adsorbed species on the surface, respectively. For Pb atom and Bi atom, E^{ads} is the energy in their stable solid states. For O atom, E^{ads} is half the energy of an oxygen molecule in a vacuum box. Thus, a negative value of E_{ads} implies that the adsorption of the species is energetically favorable. In addition, the adatom may penetrate into the substrate through substitution of the surface atoms. Here, the substitution energy[34] is calculated by

$$E_{sub} = E^{sub}_{slab} - (E_{slab} + E^{sub} - E^{Fe}), \quad (3)$$

where E^{sub}_{slab} and E_{slab} are the total energies of the Fe slab with and without one substitution species on the surface, respectively. For Pb atom and Bi atom, E^{sub} is the energy in their stable solid state. For O atom, E^{sub} is half the energy of an oxygen molecule in a vacuum box. E^{Fe} is the energy of an Fe atom in its stable solid state. Table 3 shows the adsorption energies of a Pb atom, a Bi atom or an O atom on a clean bcc Fe(100), Fe(110) and Fe(111) surface at different sites calculated with the G-NN potential together with the results obtained from density functional theory by ourselves and others.[22] Overall, the Pb, Bi and O all prefer the hollow site on the (100) surface and long bridge site on the (110) surface. However, the Pb and Bi prefer the widest hollow site on the (111) surface and the O prefers the compact bridge site. Furthermore, the adsorption energies of O atom on different Fe surfaces are much smaller than those of Pb and Bi atoms, indicating that Fe atoms prefer to bind with O atoms rather than the Pb and Bi atoms due to their large electronegativity difference. From this point of view, it is feasible to prevent dissolution by oxidation as Fe is exposed to liquid LBE. To be specific, the preferred adsorption of O atoms on Fe surfaces makes it possible for oxide formation to occur prior to the liquid LBE penetration into the Fe substrate. Moreover, compared with the most favorable adsorption energies of Pb atom and Bi atom on each surface, the most favorable adsorption energy of O atom on different Fe surfaces follows different sequences. In the cases of Pb and Bi adsorption, the adsorption energies on the Fe(111) surface are the smallest due to its loosest atomic packing among the three surfaces. However, the adsorption energy of O atom on the Fe(111) surface appears to be the highest, meaning that it is not determined by the atomic density itself. The adsorption of O atom on different Fe surfaces is more complex because the oxygen and iron interaction is more of a chemical interaction. In terms of the adsorption of O atom on different Fe surfaces, we cannot attribute simply the surface orientation dependence of adsorption energies to the differences in the atomic packing density of the surface planes. In addition, the substitution energies of Pb and Bi atoms on different surfaces are relatively small compared to their lowest adsorption energies, showing that Pb and Bi atoms prefer to substitute the surface Fe atoms rather than being adsorbed on the surface. The substitution energies of O atoms are higher, showing that O atoms prefer to be adsorbed on the surfaces rather than substitute the Fe sites. It is noted that the adsorption energy difference between the long bridge and short bridge sites on Fe(110) surface is not so large.

Table 3. Adsorption energies and substitution energies (eV) of a Pb atom, a Bi atom or an O atom on clean bcc Fe(100), Fe(110), and Fe(111) surface at different sites. H, B, LB, SB, and S represents hollow, bridge, long bridge, short bridge, and substitution sites on different surfaces, respectively, as described in Ref. [22].

	Pb (G-NN potential)	Pb (DFT present)	Pb(DFT [22])	Bi (G-NN potential)	Bi (DFT (present))	Bi(DFT [22])	O (G-NN potential)	O (DFT (present))
H(100)	–0.68	–0.80	–0.75	–1.34	–1.38	–1.36	–3.47	–3.38
B(100)	–0.23	–0.25	–0.13	–0.49	–0.57	–0.51	–3.06	–2.78
LB(110)	–0.86	–0.94	–0.91	–1.21	–1.36	–1.16	–3.21	–3.31
SB(110)	–0.85[b]	–0.84	–0.75	–1.07[b]	–1.15	–1.10	–3.01	–2.86
H(111)[a]	–1.08[d]	–0.51		–1.19	–1.07		–2.89	–2.74
B(111)	–1.17[c]	–1.32[c]	–1.04	–1.48[c]	–1.83[c]	–1.25	–3.15	–3.00
S(100)	–1.19	–1.34		–1.67	–1.69		–2.38	–2.08
S(110)	–1.02	–0.91		–1.56	–1.30		–1.24	–0.93
S(111)	–1.33	–1.40		–1.93	–1.84		–2.67	–2.57

Note: [a]H (111) represents hcp hollow site.
[b]The initial sites of the Pb and Bi atoms were set at the short bridge sites, but their final positions relaxed to long bridge sites.
[c]The initial sites of the Pb and Bi atoms were set at the bridge sites, but their final positions relaxed to fcc hollow sites.
[d]The initial site of the Pb was set at the hcp hollow site, but its final position relaxed to fcc hollow site.

As we mentioned earlier, dissolution of steel constituents and their diffusion in liquid LBE are significant corrosion process of stainless steels in liquid LBE. Diffusion of oxygen in liquid LBE is also of great importance for both probing oxygen and revealing the corrosion mechanism of the structural materials in LFR. The mutual diffusion coefficient is an important parameter to exhibit the diffusion mobility. The higher the mutual diffusion coefficient is, the greater the diffusion velocity is. In the calculation of Fe and O diffusion coefficients, 2 Fe atoms and 20 O atoms are included in the liquid LBE with 550 Bi atoms and 450 Pb atoms in a cubic cell. The mutual diffusion coefficient can be obtained by calculating the time-dependent mean-square displacement (MSD), which is a measure of the average distance that an atom/molecule travels:

$$\mathrm{MSD} = \langle |r(t) - r(0)|^2 \rangle, \tag{4}$$

where $|r(t) - r(0)|$ is the distance a single atom traveling over a time interval t, and $\langle\ \rangle$ denotes the average value of all atoms in each bin. Since the diffusion of atoms in six directions in liquid system is equivalent, according to the Stokes–Einstein relationship, the mutual diffusion coefficient D can be obtained as follows:

$$D = \lim_{t\to\infty} \frac{1}{6t} \mathrm{MSD}. \tag{5}$$

Tables 4 and 5 show the diffusion coefficients of Fe and O in liquid LBE at different temperatures by our simulations as well as reference results. It can be seen that both diffusion coefficients increase with temperatures, and our simulated results are in reasonable agreement with experimental measurements. It is worthy to note here that the number of O atoms capable of going from liquid LBE to Fe substrate side will be small in our following simulations based on the order of the diffusion coefficients shown here and the limited simulation time scale.

Table 4. Temperature dependence of the diffusion coefficients (cm^2/s) of Fe in LBE.

	G-NN potential	Experiment[35–37]
673 K	2.32×10^{-7}	3.5×10^{-7} [35]
743K	5.87×10^{-7}	7.6×10^{-7} [35]
823 K	7.56×10^{-6}	7.8×10^{-6} [36]
873 K	8.95×10^{-6}	1.2×10^{-5} [36]
923 K	9.76×10^{-6}	1.5×10^{-5} [36]
1023 K	1.20×10^{-5}	2.27×10^{-5} [37]

Table 5. Temperature dependence of the diffusion coefficients (cm^2/s) of O in LBE.

800 K (G-NN potential)	800 K (FPMD[38])	810.5 K (Experiment[39])	1000 K (G-NN potential)	1000 K (FPMD[38])	980.1 K (Experiment[39])
1.20×10^{-5}	2.18×10^{-5}	4.29×10^{-6}	4.88×10^{-5}	3.14×10^{-5}	2.96×10^{-5}

3.2. Early stage dissolution behaviors of clean bcc Fe surfaces contacting with liquid LBE-O

As mentioned above, dissolution means either dissolution of structural elements into liquid LBE or penetration of liquid LBE component into metal substrate. According to our dynamic simulations, due to the surface or near-surface Fe atoms escaping from the substrate and diffusing to the liquid, vacancies accumulate in the substrate and Pb/Bi atoms occupy these vacancies. Figure 2 shows the top view of the Fe(100)-liquid LBE-O interface at 1 ns at 873 K. It can be seen that oxygen atoms are absorbed on top of the surface, while Pb/Bi atoms occupy the vacancy site. In the case of (111) and (110) surfaces, O atoms sit on the top, and Pb or Bi atoms stay in the substitution sites, as well. It is in line with above static adsorption energy calculations.

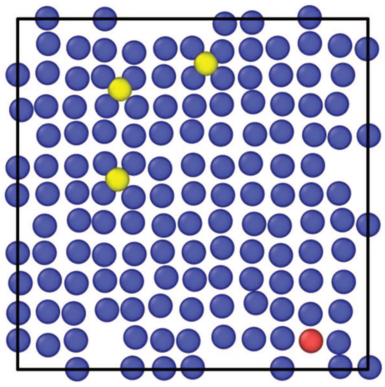


Fig. 2. Top view of bcc Fe(100)–liquid LBE-O interface at 1 ns at 873 K (red, yellow and blue balls represent Bi, O, and Fe atoms, respectively).

Leaving-Fe atoms percentage and penetrating-atoms percentage are defined to show the dissolution behavior on each surface. The leaving-Fe atoms percentage is defined as the ratio of the number of Fe atoms dissolving to the liquid side after a period of time to the initial total Fe atom number of the first layer of the Fe substrate. Similarly, the penetrating-atoms percentage is defined as the ratio of the number of Pb/Bi atoms penetrating into the Fe substrate after a period of time to the initial total Fe atom number of the first layer in the cases of (100) and (110) substrates or to the total initial Fe atoms in both first and second layers of Fe substrate near the liquid side. The difference in the definition of penetrating atoms percentage for different surface is due to the fact that Pb/Bi atoms can only penetrate into the first layer of the Fe substrate with (100) and (110) orientations, but can penetrate deeper into the second layer of Fe substrate with (111) orientation within our current simulation timescale.

The orientation and time-dependent penetrating-atoms percentage at 873 K are plotted in Fig. 3(a). The penetrating-atoms percentages are smaller than 3% for both the (100)-oriented and (110)-oriented Fe surfaces, while it is larger than 5% for the (111)-oriented Fe surface. The orientation and time-dependent leaving-Fe atoms percentages are plotted in Fig. 3(b). It shows roughly the same trend as that of the penetrating atoms. This phenomenon can be attributed mainly to the higher surface energy of the bcc Fe(111) surface and its lower surface atomic density. To be specific, at the very beginning of the oxidation and dissolution process as the clean Fe exposed to the liquid LBE-O, the surface dissolution anisotropy could be attributed to the binding energy of the surface atoms, where close packed planes tend to have higher binding energy due to their higher atomic coordination. so that the surface dissolution rates scale inversely with the atomic packing density on the surface. It is worthy of emphasizing that the presence of liquid LBE results in a higher dissolution rate of the Fe atoms than immersed in gaseous environment

and the dissolving Fe atoms could cause severe lattice distortions that are difficult to restore. Furthermore, the lattice distortion breaks the atomic bonds and make more Fe atoms get out of their lattice position and dissolve into the liquid LBE, leaving more open sites for liquid atoms to penetrate into the matrix. This recursion illustrates that dissolution plays a significant role in the corrosion behaviors of Fe exposed to the liquid LBE. It is also further noted that the severe dissolution behaviors of the (111)-oriented Fe surface will make it a weak part in the Fe material in terms of corrosion.

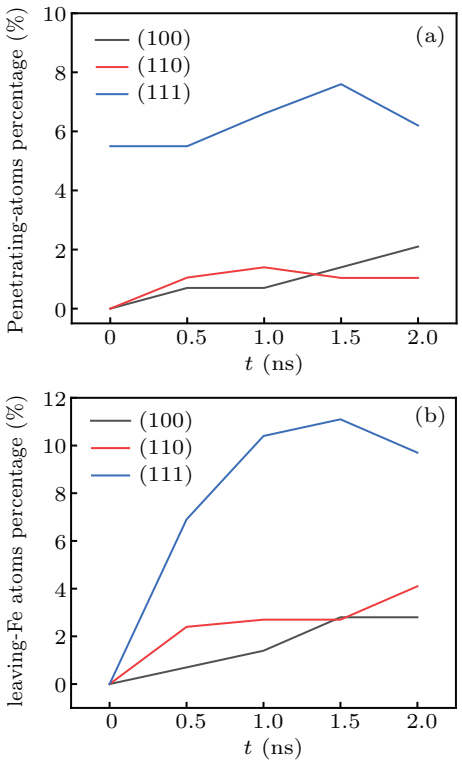


Fig. 3. Orientation and time-dependent (a) penetrating-atoms (Pb and Bi atoms) percentage and (b) leaving-Fe atoms percentage.

3.3. Early stage oxidation behaviors of clean bcc Fe surface contacting with liquid LBE-O

Currently, not much is known about the initial oxidation growth kinetics at the nanoscale. Given the great practical importance of the early stage oxidation of Fe surfaces exposed to the liquid LBE-O, an atomic level observation of the early stage oxidation process on different Fe surfaces contacting with the liquid LBE-O is the main focus in this section. Radial distribution functions (RDFs) were used to characterize the structural evolution of the three crystal surfaces during the oxidation. The RDF is defined as the probability of finding an atom at a distance r from another atom compared to a homogeneous distribution and is given as follows:

$$g(r)=\frac{V}{N_{\mathrm{A}}N_{\mathrm{B}}}\frac{1}{4\pi r^2}\left\langle\sum_{i=1}^{N_{\mathrm{A}}}n_{i\mathrm{B}}(r,\Delta r)\right\rangle. \tag{6}$$

Here, V is the volume, N_{A} and N_{B} are the numbers of A atoms and B atoms counted for the RDF; $n_{i\mathrm{B}}$ is the number of B atoms found in a shell from r to $r+\Delta r$. We have analyzed the RDF near the Fe surfaces and the results are shown in Fig. 4.

Common first nearest and second nearest neighbor distance reported for Fe–O bond are about 1.887 Å and 2.032 Å for Fe_3O_4, and 1.98 Å and 2.08 Å for α-Fe_2O_3.[40] As for FeO, its first nearest neighbor length of Fe–O bond is 1.96 Å.[40] We use the RDF profiles of the oxides to fingerprint the oxide structures formed during the early stage oxidation on the Fe crystal surfaces. In the case of Fe(100) and Fe(111), the first peak of Fe–O, locating at 1.98 Å under 873 K as shown in Fig. 4, is very close to the first nearest neighbor distance found in α-Fe_2O_3 and FeO structures. Noticeably, in the case of Fe(110), the first peak of Fe–O locating at 1.88 Å is very close to the first nearest neighbor distance found in the case of Fe_3O_4 structure. Furthermore, the overall shapes for both the Fe(100) and Fe(111) as shown in Fig. 5 are closer to the α-Fe_2O_3 structures.[23] Experimentally, iron oxides formed in liquid LBE loops have been found mainly to be Fe_3O_4 (magnetite) and sometimes α-Fe_2O_3.[41] As a matter of fact, it is far from the formation of a real oxide film with so low oxygen coverage and with so short simulation time in our study. However, during the beginning stages of iron oxidation in the liquid LBE environment at temperature of 873 K, the RDF results show that the as-formed Fe–O bonds in our simulations verge on the positions of Fe–O bonds in Fe_3O_4 and α-Fe_2O_3 structures. In other words, it shows roughly the trend towards the formation of Fe_3O_4 and α-Fe_2O_3.

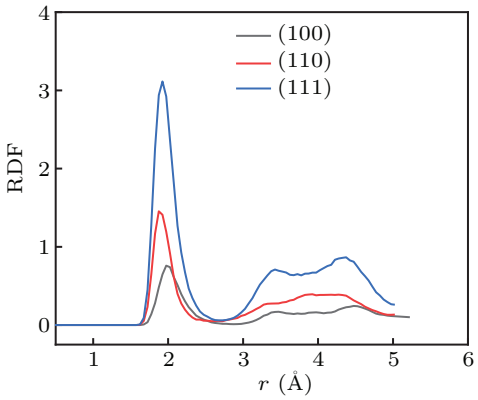


Fig. 4. Radial distribution functions for Fe–O pair obtained for Fe(100), Fe(110), and Fe(111).

In general, a crystalline oxide is expected to have well-defined sharp peaks corresponding to higher order neighbors, whereas an amorphous oxide shows a more smeared out distribution. Thus, our analyses to the higher order peaks in the Fe–O RDF suggest that the oxide formed in the case of Fe(110) and Fe(100) are amorphous in nature whereas a more crystalline oxide structure is evident in the case of Fe(111) surface as shown in Fig. 4. It is noted that orderliness of oxide film formation tendency is not incompatible with the results of the severe dissolution behaviors on the (111)-oriented surface. The presence of liquid LBE brings about great changes in the

corrosion behaviors of Fe surfaces. As presented in Subsection 3.1, in comparison with adsorption energies of Pb atom or Bi atom on the clean bcc Fe(100) and Fe(110) surfaces, the adsorption energies of atoms on bcc Fe(111) surface are relatively small, which implies that the adsorption of these species is energetically favorable on (111) surface. Meanwhile, the severe dissolution of Fe(111) surface leaves more vacancies on the Fe(111) surface. It encourages more O atoms to be adsorbed on the Fe(111) surface compared to the Fe(100) and Fe(110) surfaces. To a certain degree, at the very beginning oxidation of the Fe(111) surface, the formation of oxide is promoted and a more crystalline oxide structure is evident in the case of Fe(111) surface.

In order to further explore the orientation dependent behaviors of oxygen on the Fe surfaces, we have presented the in-plane trajectory of the O atoms on different Fe surfaces, and the results are shown in Fig. 5. When the O atoms arrive at the metal surfaces, adsorption occurs on the surfaces. Then the adsorbed O atoms will diffuse on the surface. Actually, this is the initial stage of oxidation. For example, in the case of Fe(100) surface as shown in Fig. 5(a), the adsorbed O atoms preferentially occupy the four-fold hollow sites and diffuse back and forth among these four-fold hollow sites on the surface during our simulations. The results are similar for the Fe(110) surface, where the adsorbed O atoms preferentially occupy bridge sites and diffuse back and forth among these bridge sites on the surface, too. It is noted that the O atoms movement on the (110) surface is more disordered due to the smaller adsorption energy difference between the two bridge sites. Although the Fe(111) surface is with looser atomic arrangement and it is badly damaged due to the dissolution, the diffusion behaviors of O atoms on the Fe(111) surface still show certain pattern. It may be related to the phenomenon that a more crystalline oxide structure is evident in the case of the Fe(111) surface. Moving on the plane may contribute to the formation of oxides.

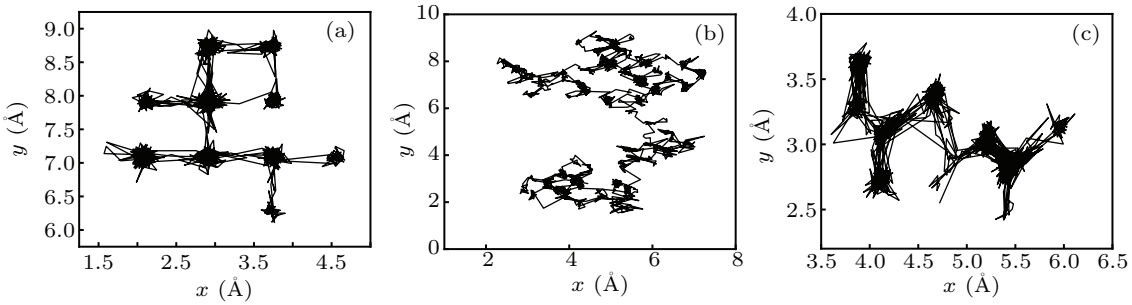


Fig. 5. In-plane trajectory of O atoms on bcc (a) Fe(100), (b) Fe(110), and (c) Fe(111).

Martinelli *et al.*[20] thought that due to outwards matrix elements diffusion from the metal to the oxidation environment, vacancies accumulated in the metal and O atoms occupied the vacancies. Our simulation shows the stage of oxidation from another perspective. At the beginning of the oxidation on different Fe surfaces, before the vacancies are formed, O atoms can occupy the hollow or bridge sites and contribute to the formation of oxides.

Comparing the MSDs of O atoms across the three surfaces, we find the MSDs to be higher in the case of Fe(110) followed by Fe(111) and Fe(100). The resultant in-plane diffusion coefficients are listed in Table 6. This is in agreement with the activation energy barrier for oxidation calculated by Su *et al.*,[23] which was found to be lowest for Fe(110) (7.44 kJ/mol) compared to the other two surfaces, 23.69 kJ/mol for Fe(100) and 19.88 kJ/mol for Fe(111). Our results suggest that the diffusivity of oxygen is strongly related to the surface orientation, being more active on the Fe(110) than on the Fe(111) and Fe(100) surfaces, which is not conducive to the nucleation of the oxide film on the (110) surface. Thus the oxide formed in the case of Fe(110) is more disorder at the beginning of oxidation as the bcc Fe contacting with liquid LBE-O.

Table 6. The in-plane diffusion coefficients (cm^2/s) of O, Pb, and Bi on different Fe surfaces at 873 K.

	O	Pb	Bi
Fe(100)	2.3×10^{-5}	2.01×10^{-8}	1.90×10^{-8}
Fe(110)	7.0×10^{-5}	3.16×10^{-8}	2.67×10^{-8}
Fe(111)	2.4×10^{-5}	1.98×10^{-8}	1.27×10^{-8}

In order to better understand the interaction process of dissolution and oxidation, we have compared the motion forms of Pb, Bi atoms and O atoms after adsorption as well by tracking the trajectories of individual Pb atom, Bi atom and O atoms at the interface. As shown above, the adsorbed O atoms preferentially occupy the hollow sites or bridge sites on the Fe surfaces and diffuse back and forth among these sites in our simulations. As shown in Fig. 6(a), trajectory of the Bi atom along z direction after adsorbed on the Fe(100) surface indicates that the Bi atoms goes through a period of thermal vibration at its adsorption site, lasting about 0.7 ns. Figure 6(b) presents the in-plane trajectory of the Bi atom during this 0.7 ns. It is clear that the displacement of Bi atom is under 0.8 Å at this stage, which confirms that this 0.7 ns is a period of thermal vibration, when the Bi atom is trapped by the Fe matrix. By tracking the trajectories of individual Pb atom and Bi atom at the interface,

we found that Pb atoms and Bi atoms diffuse slowly as they go through the period of thermal vibrations at their adsorption site. Specially, during the period of thermal vibration of Bi atoms as shown in Fig. 6, the diffusion coefficient along z direction is nearly zero, and that in the x–y plane is about 1.90×10^8 cm^2/s, which is much less than that of O atoms. Differences in the motion modes of Pb, Bi atoms and O atoms may cause dissolution and oxidation to have different effects on the Fe surfaces. Due to the longtime thermal vibrations of penetrating Bi or Pb atoms in the Fe substrate, it will cause severe lattice distortions that are difficult to restore. Furthermore, the lattice distortion may lead to atomic bonds break, which will make more Fe atoms get out of their lattice positions and dissolve into the liquid LBE, leaving more open sites for liquid atoms to penetrate into the Fe substrate. However, as far as the O atom is concerned, under our simulated conditions, the damage of O atoms to the substrate is not obvious.

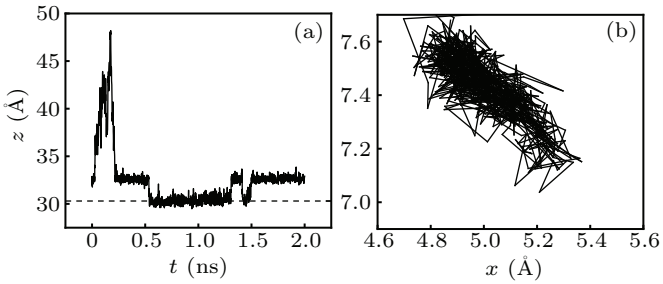


Fig. 6. Trajectories of the Bi atom (a) along z direction and (b) in the x–y plane from 0.5 ns to 1.2 ns for model system as shown in Fig. 1. The dotted line in (a) shows the boundary between liquid LBE-O and Fe substrate.

3.4. Structural changes of bcc Fe caused by oxidation and dissolution

In order to investigate the relaxation behavior of the Fe crystal planes near the surface after contacting with the LBE-O, the interlayer spacings, defined as the distance between two neighbor density peaks, of the first 8 crystal planes of Fe(110) and Fe(100) have been calculated as shown in Fig. 7. Here, the sizes of the bins used to calculate the fine-scale density are set to be 1/2000$^{\text{th}}$ of the Fe lattice constant. Due to the relatively small interlayer spacing and severe damage of the Fe(111) in the LBE-O liquid, it is hard to define the interlayer spacing of the first several crystal planes of Fe(111) as performed in the cases of Fe(100) and Fe(110). As shown in Fig. 7, surface relaxations in the Fe(100) and Fe(110) occur mainly in the first three to four crystal planes and then the interlayer spacing converges to the bulk value, 1.4175 Å for the Fe(100) interlayer spacing and 2.0046 Å for the Fe(110) interlayer spacing. The first crystal planes are basically under contraction state whether contacting or not with the liquid LBE-O. However, due to the squeeze of Pb/Bi atoms as they are contacting with the LBE-O, this effect is more obvious. All these results show that in the present simulation scale, the affected area is concentrated in the first few layers of the Fe(100) surface and Fe(110) surface.

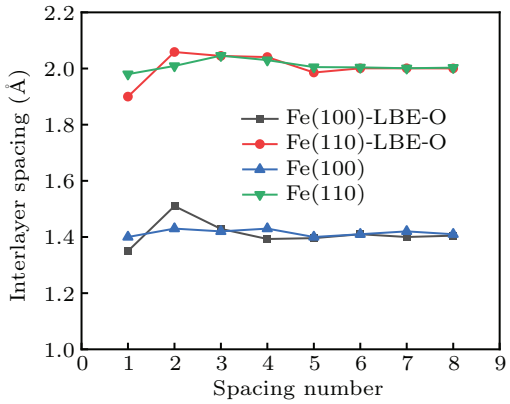


Fig. 7. Interlayer spacing of Fe(100), Fe(110), Fe(100)-LBE-O solid-liquid interface and Fe(110)-LBE-O solid-liquid interface.

In order to further explore the effect of oxidation and dissolution on the overall structure of Fe substrate, common neighbor analysis (CNA) is used to express the evolution of structure transformation. The CNA[42] is an algorithm to compute a fingerprint for pairs of atoms, which is designed to characterize the local structural environment. A cutoff distance must be chosen according to the crystal structure at hand. For bcc structures the cutoff radius should be positioned between the second and the third neighbor shells. Typically, the CNA is used as an effective filtering method to classify atoms in crystalline systems, with the goal to get a precise understanding of which atoms are associated with which phases, and which are associated with defects. The closer the CNA number is to 100%, the more crystalline the structure is. The CNA numbers for Fe surfaces are calculated for the structures snapped at 200 ps, after which these CNA numbers stay basically unchanged. As shown in Table 7, after contacting with the liquid LBE-O, the structural integrities of the (100)-oriented Fe surface and (110)-oriented Fe surface are better preserved compared to the (111)-oriented Fe surface.

Table 7. Common neighbor analyses of (100)-oriented Fe crystal, (110)-oriented Fe crystal and (111)-oriented Fe crystal.

	bcc structure
(100)	83%
(110)	77%
(111)	53%

Under our simulation conditions, the most serious damage occurs on the (111)-oriented surface due to the combined dissolution and oxidation. It should be emphasized that our simulation conditions focus on the early stage oxidation and dissolution behaviors of the clean bcc Fe contacting with the liquid LBE-O when a robust passive film does not take shape yet. It also applies to extreme conditions when the main corrosion mechanism changes from oxidation to dissolution to some degree. For example, experimental results have shown that there is a transition temperature or temperature range around

823 K with respect to steels at which the main corrosion mechanism changes from oxidation to dissolution.[43–45] Moreover, in high flow velocity liquid LBE corrosion tests, with the elapse of corrosion time, the oxide scale formed on the Fe surface tends to detach and buckle, resulting in accumulation of liquid metal in the corrosion layer. As the oxidation occurs, oxygen depletion in the liquid metal gives way to considerable Fe dissolution.[13,43] Under these circumstances, the absence of robust passive film makes dissolution dominate. The corrosion anisotropy for metals may cause unevenly distributed partial corrosion such as pitting.

3.5. Early stage dissolution and oxidation behaviors of oxygen precovered bcc Fe surface contacting with liquid LBE-O

As mentioned above, surface passivation is an effective way to mitigate corrosion. The passivation, also termed primary passivation, is a surface process occurs over timescales of 10 ms or less.[46,47] Due to the time length limitation of MD simulation, the number of O atoms going from the liquid LBE-O to the Fe substrate side is relatively small. In consequence, it is hard to get deep insight into the synergistic interaction of oxidation and dissolution in our clean surface LBE-O in nanosecond timescale simulations. Therefore, we have conducted additional calculations for oxygen precovered surfaces contacting with the liquid LBE-O at the beginning of the calculations to simulate the situation that more and more oxygen atoms go from the liquid LBE to the bcc Fe surfaces.

Coverage is defined as a ratio of the number of adsorbed O atoms to the number of Fe substrate atoms on the surface. For the dissolution and oxidation behavior of the O-precoverd bcc Fe different surfaces exposed to the liquid LBE-O, based on the above-mentioned models of clean bcc Fe-liquid LBE-O, O atoms with coverages of 0%, 12.5%, 25% and 50% distributing randomly among the preferred sites on each surface are investigated in this section.

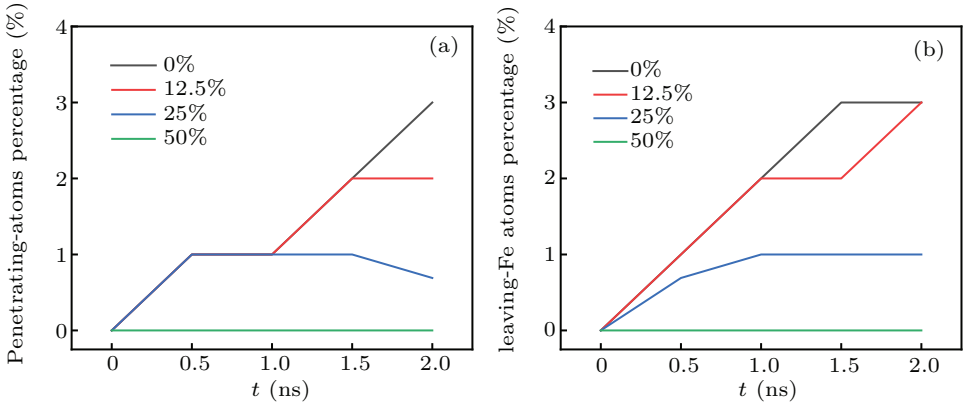


Fig. 8. Time-dependent (a) penetrating-atoms (Pb and Bi atoms) percentage and (b) leaving-Fe atoms percentage for Fe(100) with O coverage of 0%, 12.5%, 25%, and 50%.

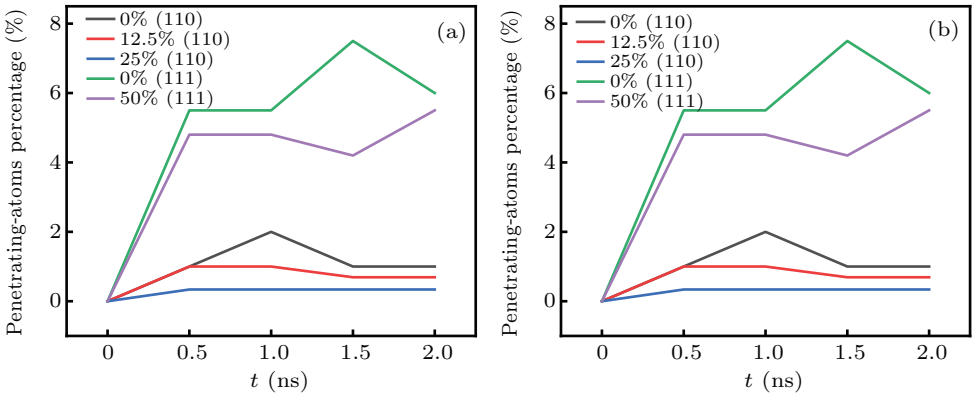


Fig. 9. Time-dependent (a) penetrating-atoms (Pb and Bi atoms) percentage and (b) leaving-Fe atoms percentage for Fe(110) and Fe(111) with different coverages of O atoms.

As shown in Figs. 8 and 9, with the increasing coverage of O atoms on the Fe(100), (110), and (111) surfaces, the penetrating-atoms percentage and leaving-Fe atoms percentage are decreasing. For the Fe(100) and Fe(110) surfaces, with a coverage of O atoms of 25%, the penetrating-atoms percentage and leaving-Fe atoms percentage are already smaller than 1%. Under these circumstances, the dissolution of structural elements into the liquid LBE and the penetration of liquid LBE components into metal substrate are difficult to happen. The O-precovered bcc Fe surfaces are of great significance to act as diffusion barriers against the dissolution of structural elements into the liquid LBE and the penetration of liquid LBE compo-

nents into the Fe substrate. These simulations confirm that passivation is an effective way to mitigate corrosion. However, in the case of Fe(111) surface, even though with a coverage of O atoms of 50%, the penetrating-atoms percentage and leaving-Fe atoms are still higher than 5% at 2 ns as shown in Fig. 9. These results show that the (111)-oriented Fe surface still undergoes the severest dissolution despite even with the oxygen coverage of 50%. In terms of CNA number, it remains unchanged for (100)-oriented and (110)-oriented Fe crystal under our simulation timescale as the precovered oxygen number increased. However, for (111)-oriented Fe crystal, it does show a slight increase to 60% with the oxygen coverage of 50%.

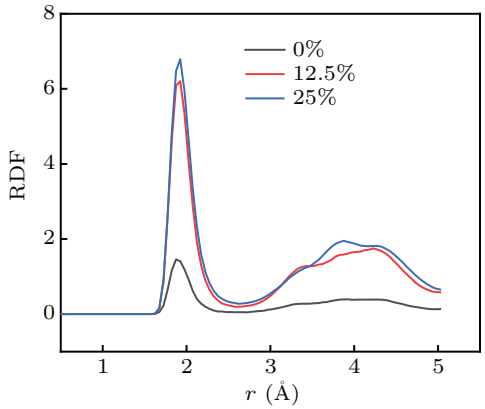


Fig. 10. Radial distribution functions for Fe–O pair obtained for Fe(110) surfaces with O coverage of 0%, 12.5%, and 25%.

Table 8. Diffusion coefficients (cm^2/s) of O on different Fe surfaces with different oxygen coverages.

	O diffusion coefficient (cm^2/s)
Fe(100) 0%	2.3×10^{-5}
Fe(100) 12.5%	1.5×10^{-5}
Fe(100) 25%	7.5×10^{-6}
Fe(100)50%	6.4×10^{-6}
Fe(110) 0%	7.0×10^{-5}
Fe(110) 12.5%	5.0×10^{-5}
Fe(110) 25%	2.8×10^{-5}
Fe(111) 0%	2.4×10^{-5}
Fe(111) 50%	1.8×10^{-5}

In terms of oxidation on the clean bcc Fe surfaces, the oxide formed in the case of Fe(110) is more disordered than that of the Fe(100) and Fe(111). Here, we explore the radial distribution functions (RDFs) of Fe–O in the case of Fe(110) with different oxygen coverages. As shown in Fig. 10, with the increasing oxygen coverage, it starts to show higher order peaks. However, the overall shapes are still more disordered than that of Fe(100) and Fe(111). We may attribute this disordered structure to the fast in-plane movement of oxygen atoms. Furthermore, it is still far from the formation of a real oxide film with so low oxygen coverage.

The diffusion coefficients (cm^2/s) of O on different Fe surfaces with different oxygen coverages are listed in Table 8. Overall, the oxygen diffusion coefficient on (110) surface is higher than those on (100) and (111) surfaces. In addition, the oxygen diffusion slows down with the increasing coverage of oxygen on all Fe surfaces, which will benefit the formation of oxide film. It is worthy to note that the decrease of the oxygen diffusion coefficients (cm^2/s) on the Fe(111) surface with different coverages of oxygen atoms is not so evident, which can be attributed to the open atomic packing on this surface.

4. Discussion

Limited by experimental technique and the almost instantaneous time scale of oxidation process, experimental research on influences of the crystal orientation is rare under the liquid LBE environment. In particular, most of the liquid LBE corrosion experiments were carried out for more than 100 hours. At this time scale, the oxide film could grow to micron level in thickness. The microscopic orientation effect is difficult to observe under this time scale. However, many macroscopic experimental observations may be attributed to the surface orientation dependent anisotropy of corrosion. For example, in our team's previous experimental research,[48] we found that the oxide film on the side close to the substrate was extremely uneven. In addition, there is no specific reason for the pitting phenomenon observed in the experiments as reported in Refs. [49,50]. The different oxidation and dissolution behaviors found in our computational simulations for the different orientations may be an important reason for the above experimental phenomena.

As for dissolution, the Fe(111) surface goes through a stronger dissolution process due to its lower atomic density compared to that of the (100) and (110) surfaces. However, for the early stage oxidation, it is more complicated. At the beginning of the stage, the number of O atoms going from liquid LBE to Fe substrate side is relatively small and the reaching surface oxygen jump rapidly among different adsorption sites on the Fe surfaces. The simulations of O-precovered bcc Fe contacting with liquid LBE-O show that the oxygen diffuse more and more slowly as the coverage of oxygen on the bcc Fe surfaces keep increasing. In reality, the number of oxygen atoms reaching the Fe surfaces is determined by the oxygen concentration in the LBE-O and the corrosion time length. Therefore, at the beginning of the corrosion process, it is unsurprised to see that the absorbed oxygen atoms on the surfaces are active and jump around their preferred adsorption sites, which would prevent the nucleation of the oxide film. However, with the increasing coverage of oxygen on the bcc Fe surfaces, oxygen atoms diffuse more and more slowly, which gradually promotes the formation of oxide film.

Although the Fe(111) surface with looser atomic arrangement is badly damaged due to dissolution, the diffusion behaviors of O atoms on Fe(111) surface still show certain pattern. It may be related to the phenomenon that a more crystalline

oxide structure is evident in the case of Fe(111) surface. Comparing the MSDs of O atoms across the three surfaces, we find the MSDs to be higher in the case of Fe(110) followed by Fe(111) and Fe(100) with a more disordered oxide formed on the Fe(110) at the beginning of oxidation as bcc Fe contacting with liquid LBE-O. That is, the more active oxygen on the Fe(110) surface indicates that it is more difficult to the nucleation of oxide film on (110) surface than on the (100) and (111) surfaces. Therefore, the resultant overall corrosion behavior is determined by the delicate balance between dissolution and oxidation, as shown by the overall structure changes characterized by the CNA listed in Table 7. Under our simulation conditions, the intrinsic degradation mechanism can be explored. This conservative consideration is essential in the sense that protective surface oxide scales can be damaged somehow in service, which will lead to direct exposure of the matrix to corrosive liquid LBE, especially in crevices and occluded regions where dissolved oxygen could be very low.

Furthermore, as reported in literature, Fe surface oxidation in gaseous medium[1–4,6,51] does show that the structure of the oxide film grown on different orientations is different. Although our simulation of Fe contacting with the liquid LBE-O is far from the formation of real oxide film with so low oxygen coverage and so short simulation time, we do find a rhombus Fe and O arrangement on the bcc Fe(111) surface, showing the trend toward the formation of hexagonal structure oxide Fe_2O_3.

5. Conclusions

Using classical MD simulation with the G-NN potential, a machine-learning interatomic potential, we have performed detailed atomic-level simulations of early stage oxidation and dissolution behaviors of the clean and O-precovered bcc Fe surfaces contacting with liquid lead-bismuth eutectic, and found that the oxidation and dissolution behaviors of bcc Fe are strongly correlated to its surface orientation. As for dissolution, the Fe(111) surface goes through a stronger dissolution process compared to the (100) and (110) surfaces. In addition, with the increasing oxygen coverage on the surfaces, the dissolution process is largely inhibited. Under the given oxidation condition, the diffusion rate of O atoms has been found to be fastest on the Fe(110) compared to the other surfaces, and slow down with the increase of oxygen coverage on all surfaces. At the beginning of early stage oxidation, the as-formed Fe–O pairs on Fe(110) and Fe(100) are amorphous in nature whereas more crystalline on Fe(111) surface. It is the delicate balance between oxide growth and metal dissolution that leads to the observed corrosion anisotropy for bcc Fe contacting with liquid LBE-O. With combined oxidation and dissolution under our simulation conditions, we found that the corrosion rate of bcc Fe in liquid LBE-O scaled with surface crystallographic orientations as $\{100\} \approx \{110\} < \{111\}$. Our current study confirms that a passive oxide film is an effective way to mitigate corrosion of Fe in liquid LBE.

Acknowledgements

We deeply appreciate Professor Zhipan Liu and Professor Cheng Shang at Fudan University for their help in training the quaternary G-NN potential used in our MD simulations. This work was supported by the National Natural Science Foundation of China (Grant No. U1832206).

References

[1] Parihar S S, Meyerheim H L, Mohseni K, Ostanin S, Ernst A, Jedrecy N, Felici R and Kirschner J 2010 *Phys. Rev. B* **81** 075428
[2] Soldemo M, Lundgren E and Weissenrieder J 2016 *Surf. Sci.* **644** 172
[3] Soldemo M, Niu Y, Zakharov A, Lundgren E and Weissenrieder J 2015 *Surf. Sci.* **639** 13
[4] Qin F, Magtoto N P, Garza M and Kelber J A 2003 *Thin Solid Films* **444** 179
[5] Zhang L, Szpunar J A, Dong J, Oj O A and Wang X 2018 *Metall. Mater. Trans. B Process Metall. Mater. Process. Sci.* **49** 919
[6] Gray J J, Dasher B S and Orme C A 2006 *Surf. Sci.* **600** 2488
[7] Dong S D, Chen X, Gussev M, Leonard K and Sant G 2010 *Mater. Des.* **191** 108583
[8] Stephan-Scherb C, Menneken M, Weber K, Jacome LA and Nolze G 2020 *Corrosion Sci.* **174** 108809
[9] Alemberti A 2016 *Engineering* **2** 59
[10] Lorusso P, Bassini S, Del Nevo A, Di Piazza I, Giannetti F, Tarantino M and Utili M 2018 *Prog. Nucl. Energy* **105** 318
[11] Lillard R S and P A Pint 2020 *Comprehensive Nuclear Materials* (Amerstadam: Elsevier) pp. 1–32
[12] Concetta F 2015 *Handbook on Lead-bismuth Eutectic Alloy and Lead Properties, Materials Compatibility, Thermal-hydraulics and Technologies* (Nuclear Energy Agency) pp. 431–453
[13] Martinelli L, Ginestar K, Botton V, Delisle C and Balbaud-Célériera F 2020 *Corrosion Sci.* **176** 108897
[14] Lambrinou K, Charalampopoulou E, Tom V, Delville R and Schryvers N 2017 *J. Nucl. Mater.* **490** 9
[15] Schroer C, Wedemeyer O, Novotny J, Skrypnik A and Juergen K 2014 *Corrosion Sci.* **84** 113
[16] Zhang J S, Hosemann P and Maloy S 2010 *J. Nucl. Mater.* **404** 82
[17] Zhang J S and Li N 2007 *Corrosion Sci.* **49** 4154
[18] Gong X, Chen J J, Xiang C Y, Yu Z Y., Gong H W and Yin Y 2021 *Corrosion Sci.* **183** 109346
[19] Xiao J, Gong X, Xiang C Y, Yu Z Y, Wang H, Zhao K, Liu C H, Zhou H, Qiu Y and Yin Y 2021 *J. Nucl. Mater.* **549** 152852
[20] Martinelli L, Balbaud-C F, Terlain A, Delpech S, Santarini G, Favergeon J, Moulin G, Tabarant M and Picard G 2008 *Corrosion Sci.* **50** 2523
[21] Zhang J S and Li N 2008 *J. Nucl. Mater.* **373** 351
[22] Xu Y C, Song C, Zhang Y, Liu C S, Pan B C and Wang Z G 2014 *Phys. Chem. Chem. Phys* **16** 16837
[23] Subbaraman R, Deshmukh S A and Sankaranarayana S K R S 2013 *J. Phys. Chem. C* **117** 5195
[24] Zhou T, Gao X, Ma Z W, Chang H L, Shen T L and Wang Z G 2021 *J. Nucl. Mater.* **555** 153107
[25] Kang P L, Shang C and Liu Z P 2020 *Acc. Chem. Res.* **53** 2119
[26] Shang C, Zhang X J and Liu Z P 2014 *Phys. Chem. Chem. Phys* **16** 17845
[27] Thompson A P, Aktulga H M, Berger R, Bolintineanu D S, Brown W M, Crozier P S, Veld P J, Kohlmeyer A, Moore S G, Nguyen T D, Shan R, Stevens M, Tranchida J, Trott C and Plimpton S J 2021 *Comput. Phys. Commun.* **271** 108171
[28] Pablo Palafox-Hernandez J and Laird B B 2010 *Acta Mater.* **59** 3137
[29] Forti M, Alonso P R, Gargano P H, Balbuena P B and Rubiolo G H 2016 *Surf. Sci.* **647** 55
[30] Pearson W B 1967 *A Handbook of Lattice Spacings and Structures of Metals and Alloys* (New York: Pergamon Press) pp. 20–50

[31] Zuo E X, Dou X L, Chen Y Y, Zhu W J, Jiang G, Mao A J and Du J G 2021 *Surf. Sci.* **712** 121880
[32] Huang Y, Hu C W, Xiao Z G, Gao N, Wang Q T, Liu Z X, Hu W Y and Deng H Q 2022 *Appl. Surf. Sci.* **580** 152300
[33] Boer F R, Boom R, Mattens W C M, Miedema A R and Niessen A K 1988 *Cohesion in Metals: Transition Metal Alloys* (Amerstadam: Elsevier)
[34] Yin H, Wu Y L, Hou J T, Yan X R, Li Z H, Zhu C W, Zhang J, Feng X G, Tan W F and Liu F 2020 *Chem. Geol.* **532** 119378
[35] Balbaud-Célérier F and Terlain A 2004 *J. Nucl. Mater.* **335** 204
[36] Banerjee S 1974 *Proceedings of the Fifth International Congress on Metallic Corrosion* Tokyo, Japan
[37] Gao Y, Takahashi M and Nomura M 2015 *Mech. Eng. J.* **2** 15-00149
[38] Li D D, Song C, He H, Liu C S, Pan B C and Wu Y 2013 *J. Nucl. Mater.* **437** 62
[39] Ganesan R, Gnanasekaran T and Srinivasa R S 2006 *J. Nucl. Mater.* **349** 133
[40] Sendja B T, Castillo N and Portales R L 2021 *Physica B* **617** 413128
[41] Shi Q Q, Liu J, Luan H, Yang Z, Wang W, Yan W, Shan Y and Yang K 2015 *J. Nucl. Mater.* **457** 135
[42] Honeycutt J D and Andersen H C 1987 *J. Phys. Chem.* **91** 4950
[43] Yeliseyeva O, Tsisar V and Benamati G 2008 *Corrosion Sci.* **50** 1672
[44] Benamati G, Fazio C, Piankova H and Rusanov A 2002 *J. Nucl. Mater.* **301** 23
[45] Gómez Briceo D, Crespo L S, Martn Muoz F J and Arroyo F H 2002 *J. Nucl. Mater.* **303** 137
[46] Xie YS, Artymowicz D M, Lopes P P, Aiello A, Wang D, Hart J L, Anber E, Taheri M L, Zhuang H L Newman R C and Sieradzki K 2021 *Nat. Mater.* **20** 789
[47] Bastek P D, Newman R C and Kelly R G 1993 *J. Electrochem. Soc.* **140** 1884
[48] Ma Z W, Shen T L, Wang Z G, Zhou T, Gao X and Chang H L 2022 *Appl. Surf. Sci.* **578** 151910
[49] Tsisar V, C. Schroer C, Wedemeyer O, Skrypnik A and Konys J 2016 *J. Nucl. Mater.* **468** 305
[50] Tsisar V, Schroer C, Wedemeyer O, Skrypnik A and Konys J 2017 *J. Nucl. Mater.* **494** 422
[51] Davies R, Edwards D, Grafe J, Gilbert L, Davies P, Hutchings G and Bowker M 2011 *Sur. Sci.* **605** 1754